Received: 12 November 2024 | Revised: 21 May 2025 | Accepted: 4 July 2025

DOI: 10.1002/suco.70248

ARTICLE

fib CEB-FIP WILEY

RC beam-column element for simulating nonlinear shear-flexural behavior

L. M. Gil-Martín | E. Hernández-Montes

Department of Structural Mechanics, University of Granada (UGR), Campus Universitario de Fuentenueva s/n, Granada, Spain

Correspondence
E. Hernández-Montes, Department of Structural Mechanics, University of Granada (UGR), Campus Universitario de Fuentenueva s/n, 18072 Granada, Spain.
Email: emontes@ugr.es

Abstract

This paper presents a precise and straightforward solution for simulating the behavior of reinforced concrete (RC) beam-column elements subjected to bending and shearing forces. The solution is compatible with the fiber element formulation used within object-oriented software frameworks like OpenSees. The solution applies to both elastic and plastic deformation domains. In order to validate the effectiveness of the beam-column element proposed, a benchmark test available in the literature has been employed.

KEYWORDS

fiber elements, performance-based design, RC beam-column elements, shear deformation

1 | INTRODUCTION

1.1 | Background and motivation

Several decades ago, the need for performance-based approaches in seismic design grew significantly in response to the substantial damage and economic losses caused by moderate earthquakes, particularly those resulting from the Loma Prieta, Northridge, and Hyogo-Ken Nambu events. This realization triggered the development of displacement-based methods for seismic design and evaluation, as noted in various studies.[1–3]

In order to support the development and application of robust numerical models for simulating inelastic structural responses, the Pacific Earthquake Engineering Research Center (PEER) introduced OpenSees (Open System for Earthquake Engineering Simulation), an open-source, object-oriented software framework (opensees.berkeley.edu). This framework includes a comprehensive suite of modules designed to facilitate the implementation of models and simulation techniques for both structural and geotechnical earthquake engineering. For the analysis of reinforced concrete (RC) structures, OpenSees uses fiber elements as a mathematical method to integrate cross-sectional responses and updates the relationships between bending moments, axial force, and curvature in a stepwise manner. Fiber elements effectively capture the nonlinear behavior of materials, making them suitable for modeling RC structures subjected to seismic events. However, the usefulness of these elements is limited when accounting for the interaction between axial-flexural and shear behavior.[4] Recently, new elements for RC columns and walls have been developed using OpenSees to address this interaction.[5]

Numerous studies in the literature have sought to improve the understanding of shear-bending interaction. These works focus on various approaches, including finite element formulations,[6] analytical models,[7] RC walls,[8] and fiber element models.[9]

Building on the concept of effective shear strain (γ_{eff}), a computational beam-column element with shear fibers has been formulated to capture shear-bending interaction.

The model is robust, visually intuitive, and applicable to both fixed and rotational compression field models. It employs coupled stiffness using FE theory while remaining uncoupled in failure mode, effectively addressing shear behavior in fiber beam-column elements. By incorporating shear deformation, it can detect if shear failure appears before bending failure. A detailed benchmark test is analyzed in Section 5.

This compact RC beam-column element has been designed for performance-based seismic design and evaluation across elastic and plastic domains.

1.2 | Objective of the study

Building on the finite element formulation of the Timoshenko beam and a quasi-Timoshenko model previously developed by the authors,[10] this work introduces a new RC beam-column element that is applicable in both elastic and plastic domains. Equilibrium relations of bending moments, forces, and curvatures are computed by using the numerical integration of the cross-sectional response. Additionally, a novel shear cross-section concept is introduced to calculate the relationship between shear force and shear strain, improving visualization and accuracy. The resulting beam-column element effectively simulates the bending and shear behavior of RC elements, advancing current methods for design and evaluation.

2 | THEORETICAL BACKGROUND AND BASIS FOR THIS STUDY

The formulation by Popovics et al. is used[11] for modeling concrete behavior, while the confinement effect is incorporated using the mechanical model created by Mander et al.[12] The steel model for reinforcing bars is bilinear, with a 1% strain-hardening ratio. The theoretical foundation of this new element is based on the Timoshenko beam, as detailed in section 39 of Timoshenko's book,[13] with its linear formulation refined by Reddy as a finite element.[14] The relationship between shear strain and shear reinforcement is derived from the quasi-Timoshenko beam model developed by the authors,[10] which is based on the truss model proposed and validated by Ueda.[15]

Both models[10,15] support the idea that shear deformation is negligible when compared to bending deformation provided that the shear reinforcement remains in the elastic range. However, once the shear reinforcement yields, shear deformation becomes significant.

In this study, the strut angle is determined by using the assumption that cracks align with the principal compression stress direction once the tensile strength of concrete is exceeded,[16] which is physically sound for the considered study case. However, alternative compression field theories[17] or[18] may also be considered, which account for concrete softening and/or tension stiffening.[19]

3 | ANALYTICAL MODELS: A DETAILED DESCRIPTION

This study employs a finite element-based formulation to model bending and shear deformations[14] and applies it to RC beam-column elements, considering both longitudinal and transverse reinforcement layouts. In order to ensure a self-contained document with uniform notation, Appendix A summarizes the development of the Timoshenko beam-column finite element. This formulation is applicable, in a stepwise manner, across both elastic and plastic deformation ranges. The NEHRP Seismic Design Technical Brief[20] classifies the most commonly used beam-column element models (Figure 1). The methodology proposed is straightforward and well-suited for scenarios involving distributed plasticity, particularly with fiber elements (or fiber sections), as shown in case (d) of Figure 1.

3.1 | The elastic beam-column element for bending and shear deformation

In the matrix representation of the behavior of a beam-column element, the element stiffness matrix $\mathbf{k}$ connects the nodal displacement vector $\mathbf{d}$ to the nodal force vector $\mathbf{f}$ (see Figure 2). For a plane beam-column element with three degrees of freedom (DOF) per node, the stiffness matrix formulation is as follows:

$$\begin{aligned} \mathbf{f} &= \mathbf{k}\mathbf{d} \\ \mathbf{f}^T &= \left[N_i, V_i, M_i, N_j, V_j, M_j\right] \\ \mathbf{d}^T &= \left[u_i, v_i, \theta_i, u_j, v_j, \theta_j\right] \end{aligned} \tag{1}$$

$\mathbf{K}$ matrix (Equation (A19)) is derived in the appendix using a finite element formulation that accounts for both bending and shear deformations. Several finite beam elements exist in the literature that consider the Timoshenko beam theory (TBT). Each of these elements differs from the others in the choice of the interpolation functions used for transverse deflection and rotation; in this work, Equations (A10) and (A11) are used.[14]

The stiffness matrix of the structure, $\mathbf{K}$, is obtained by assembling the $\mathbf{k}$ matrices of all its elements.

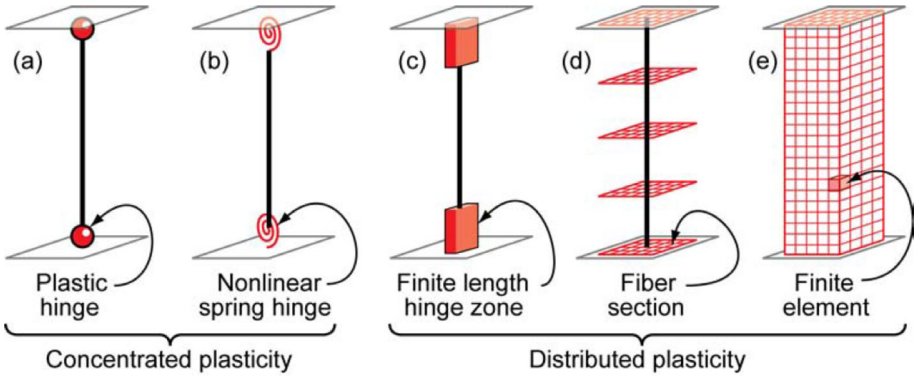

FIGURE 1 Idealized models of beam-column elements. NEHRP Seismic Design Technical Brief No 4.[20]

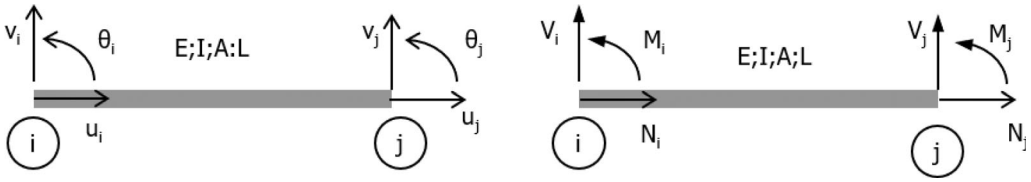

FIGURE 2 Nodal displacements and nodal forces in a planar beam-column element.

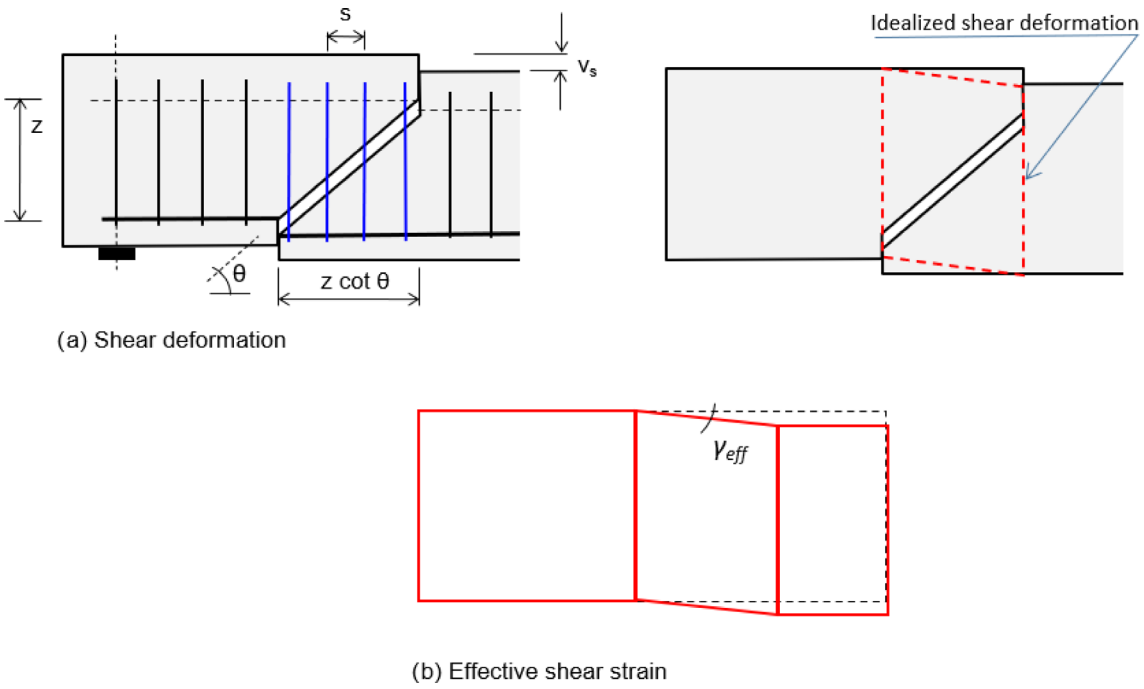

FIGURE 3 Effective shear strain.

3.2 | The quasi-TBT for RC beam-column elements

In the beam-column RC element model considered in Reference [10] shear strain is caused by the deformation of the shear reinforcement and the effective area of concrete surrounding the reinforcement. Without any loss of generality, the shear reinforcement is considered to be perpendicular to the centerline of the non-deformed beam-column element. An effective shear strain (γ_{eff}) is defined, which is a function of the angle of the crack (θ), the lever arm (z), and the elongation of the shear reinforcement (v_s), see Figure 3. During the considered shear deformation, all the

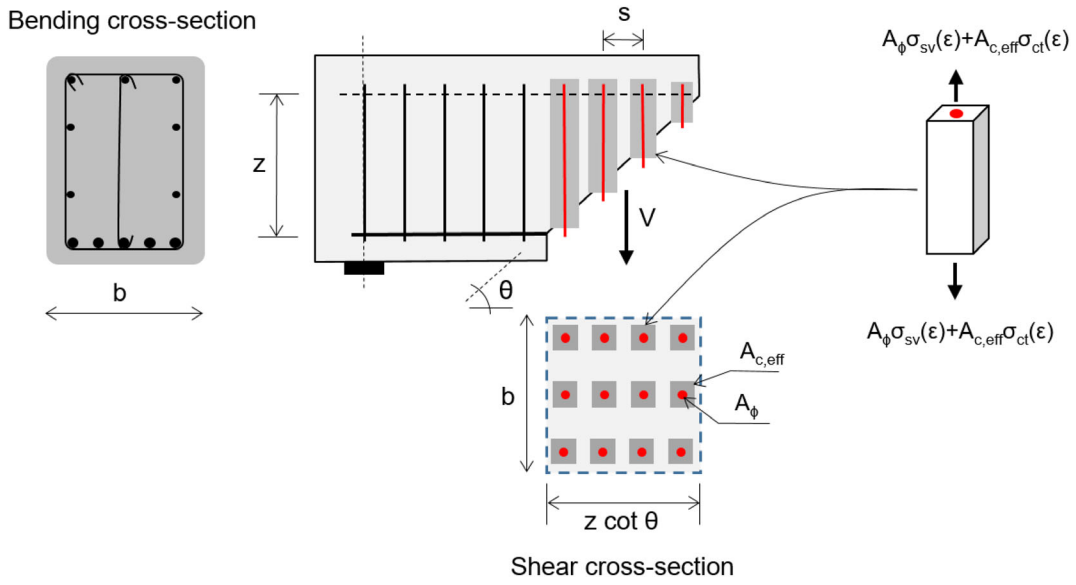

FIGURE 4 Response of shear reinforcement.

stirrups involved (shown in blue) deform by the same amount (v_s).

In accordance with traditional nomenclature, the authors have used θ as the rotational degree of freedom in the nodes, and also as the angle of the crack in concrete elements. Readers will have to differentiate between the two meanings by considering the context in which they are presented.

The procedure proposed applies to both rotating and fixed-angle models. In the rotating angle model, the angle must be recalculated at each loading step using any available compression field theories from the literature.[16] A previously developed example of a four-point bending test demonstrates the good performance of this quasi-Timoshenko beam model.[10]

$$\left.\begin{array}{l}\gamma_{\text{eff}}=\dfrac{v_s}{z\cot\theta}\\ \varepsilon=\dfrac{v_s}{z}\end{array}\right| \rightarrow \varepsilon=\gamma_{\text{eff}}\cot\theta \qquad (2)$$

As previously mentioned, shear deformation in RC beam-columns results from the elongation of the tensioned shear reinforcement, specifically the deformation of the stirrup legs (see Figure 3). Additionally, the contribution of the surrounding concrete in tension, within the effective area $A_{c,eff}$, is considered (tension stiffening effect), as shown in Figure 4. As stated by the new EN 1992,[21] the effective area of concrete in tension perpendicular to the bar is limited to a distance from the bar that is smaller than 5ϕ, with ϕ representing the diameter of the bar. In this work, the linear approximation for tension stiffening proposed by Hdz-Gil and Hernández-Montes[22] is used. Since this model was calibrated using the approximate deflection expressions from current standards, it also accounts for the bond-slip effect within the beam-column element. However, it does not consider the bond-slip that occurs at the element ends, such as at the end of a cantilever beam, like the one analyzed in Section 5.

Similar to the traditional cross-section used for bending, a shear cross-section can be defined (see Figure 4). This shear cross-section includes all the stirrup legs and the surrounding effective concrete areas that contribute to shear deformation over a length of $z\cot\theta$.

In Figure 3a, as the right side of the beam moves downward as a result of shear deformation, all the blue stirrup legs elongate. Due to tension stiffening, the effective cross-section of each leg includes both the reinforcing bar and the surrounding concrete. Consequently, the shear deformation involves the combined cross-sections of all the stirrup legs, forming the shear cross-section, as illustrated in Figure 4.

It is important to note that, due to the relatively short length of the stirrup legs (approximately z), the deformation, during shear failure, before bar break, is quite small. Consequently, in order to prevent shear failure and promote bending failure, American codes (ACI-318) use a lower safety factor (ϕ factor) for shear failure compared to that used for bending. However, having a tool capable of capturing the shear response, especially in performance-based design, is still an essential element.

If the number of legs of each stirrup is denoted as n_l (e.g., $n_l = 3$ in Figure 4), the area of the transverse reinforcing bars is $A_\varnothing$, and the effective area surrounding the bar contributing to tension is $A_{c,eff}$, the equilibrium of vertical forces results in the following shearing force[10]:

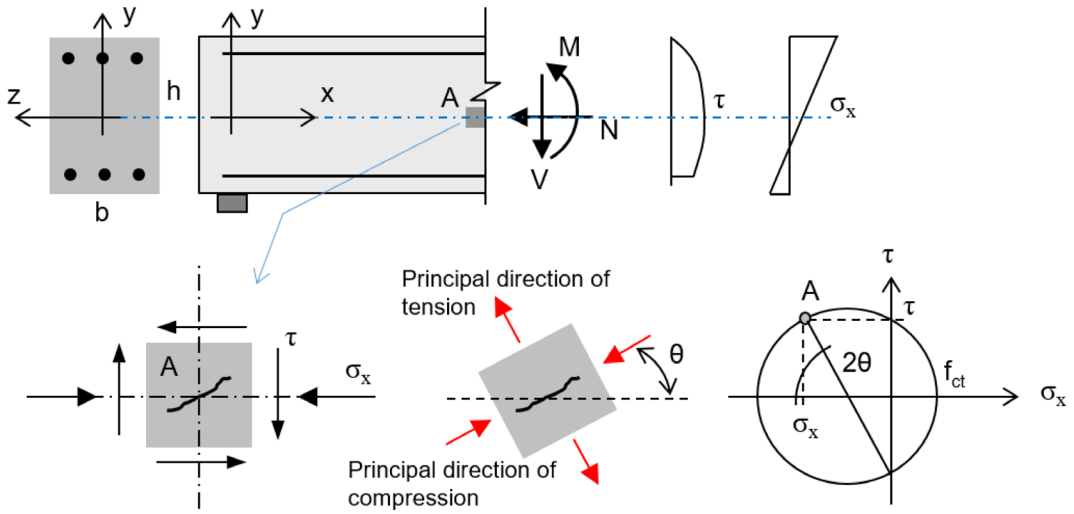

FIGURE 5 Angle of the principal direction of compression (θ).

$$V(\gamma_{\text{eff}}) = \frac{z\cot\theta}{s} n_l \left(A_\phi \sigma_{sv}[\gamma_{\text{eff}}\cot\theta] + A_{c,\text{eff}}\sigma_{ct}[\gamma_{\text{eff}}\cot\theta]\right) \tag{3}$$

The first and second terms on the right of the equation correspond to the contributions of steel and concrete, respectively.

3.3 | Struts angle, θ

The θ angle can be deduced from any of the compression field theories.[10] A sound simplification can be made in the case of columns, where shear cracks can appear without any prior concrete deterioration. This phenomenon occurs because, unlike in beams, in which bending causes concrete to crack, the concrete sections of columns are typically fully compressed before shear cracking occurs. In the case of columns, θ is adopted as the angle of the principal direction of compression at the centerline of the beam-column element when a crack occurs (see Figure 5).

The Mohr circle in Figure 5 enables the shear stress that induces tensile cracking in concrete (Equation (4)) and the crack angle (θ) (Equation (5)) as a function of the axial force, N to be calculated. Equation (5) clearly shows that when $N = 0$, $\theta = 45°$, and as the value of N increases, the θ angle decreases from 45°.

$$f_{ct} = \sqrt{\left(\frac{\sigma_x}{2}\right)^2 + \tau^2} - \frac{\sigma_x}{2} \rightarrow \tau = \sqrt{f_{ct}^2 + f_{ct}\sigma_x} = \sqrt{f_{ct}^2 + f_{ct}\frac{N}{A}} \tag{4}$$

$$\tan(2\theta) = \frac{2\tau}{\sigma_x} = \frac{2\sqrt{f_{ct}^2 + f_{ct}\frac{N}{A}}}{\frac{N}{A}} \tag{5}$$

Figure 6 illustrates the influence of the axial load on the angle of a crack. In the highlighted column, the first crack appeared during an interstory movement to the right when the column was fully compressed. The crack (and the principal direction of compression) inclined toward the vertical axis (see Figure 6 and Equation (5)). After this crack had occurred, the stress state in the concrete changed, and the axial force was probably primarily withstood by the rebars. From that point onward, the concrete was no longer subjected to axial force. Consequently, during a subsequent movement to the left, the crack orientation was closer to 45°.

Detailed examples of how the angle of the crack is calculated by applying different compression field theories can be found in References [10,16].

4 | THE RC BEAM-COLUMN ELEMENT

Figure 7 presents the flowchart outlining the construction of the RC beam-column element for both elastic and plastic deformations in bending and shear. A nonlinear concrete model is used, incorporating tension stiffening, along with a bilinear model for steel. It is a control-displacement element, as the flow chart starts with a displacement increment at i degree of freedom ($\Delta\mathbf{D}_i$). Linear elastic formulation is used in each of the displacement steps considered (i.e., $\Delta\mathbf{F}=\mathbf{K}\ \Delta\mathbf{D}_i$). Matrix $\mathbf{K}$ is the assemblage of $\mathbf{k}$ element matrices (defined in Equation (-A19)), and $\mathbf{K}_B$ is the stiffness bending matrix, that is, when shear deformation is not considered (or equivalently, when the ratio between flexural and shear stiffnesses is zero, see Equation (A13) for $\beta = EI/GA\kappa_s = 0$).

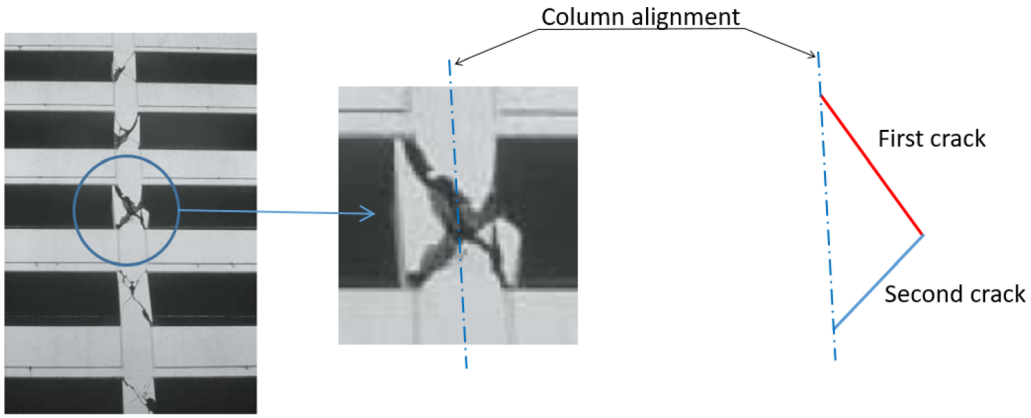

FIGURE 6 A parking structure during the Northridge earthquake on January 17, 1994.

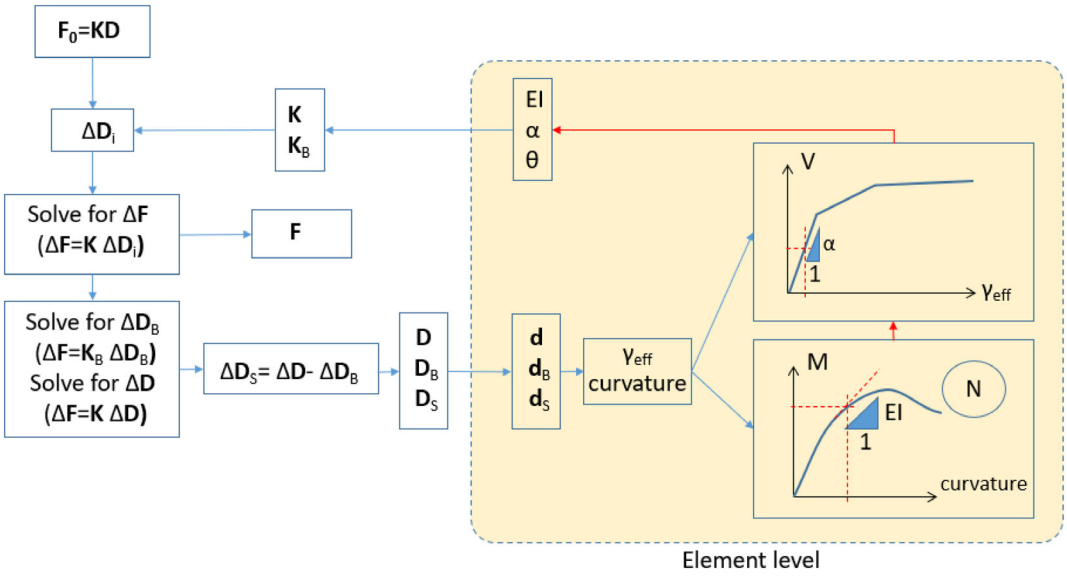

FIGURE 7 Flow chart for the construction of the RC beam-column element.

In Equation (A5), $GA\kappa_s$ (or shear stiffness) represents the slope of the shear force versus shear strain graph (V–γ). Figure 8 provides an example of the V–γ_{eff} graph from,[10] which illustrates three stages: pre-cracking, pre-yield, and post-yield. Both the tension stiffening of concrete and steel plasticization are considered in the construction of Figure 8, using C25 concrete and B400 steel. In the quasi-Timoshenko beam model proposed for the RC beam-column element, the γ_{eff} effective shear strain is considered (see Equation (3)) instead of γ, with the slope of the V–γ_{eff} graph denoted as α (i.e., $\alpha = dV/d\gamma_{eff}$), as shown in Figures 7 and 8. A crack angle (θ) of 45° was assumed in this example.

A numerical approach for considering the variation of the coefficients of matrix $\mathbf{k}$ in Equations (1) and (A19) involves dividing the displacement into multiple steps, considering the variation of the EI and $GA\kappa_s$ coefficients from one step to the next:

$$\mathbf{\Delta f} = \mathbf{k}\,\mathbf{\Delta d} \tag{6}$$

As EI and $GA\kappa_s$ are functions of the actions (i.e., $EI = EI(N, M)$ and $GA\kappa_s = GA\kappa_s(V)$), they vary throughout the displacement process.

In Equation (A4), EI (or bending stiffness) represents the slope of the moment-curvature diagram, as curvature, by definition, is the variation in rotation caused by bending. Moment-curvature diagrams are constructed for constant values of the N axial force. Numerical processes equivalent to the use of moment-curvature graphs can be employed (i.e., equilibrium and compatibility equations at a cross-sectional level). However, in this study, moment-curvature diagrams are used for better visualization; see Figure 7. Moreover, concrete tension stiffening and softening, confinement effects, bond-slip, and steel plasticization are considered to obtain moment-curvature diagrams.[16]

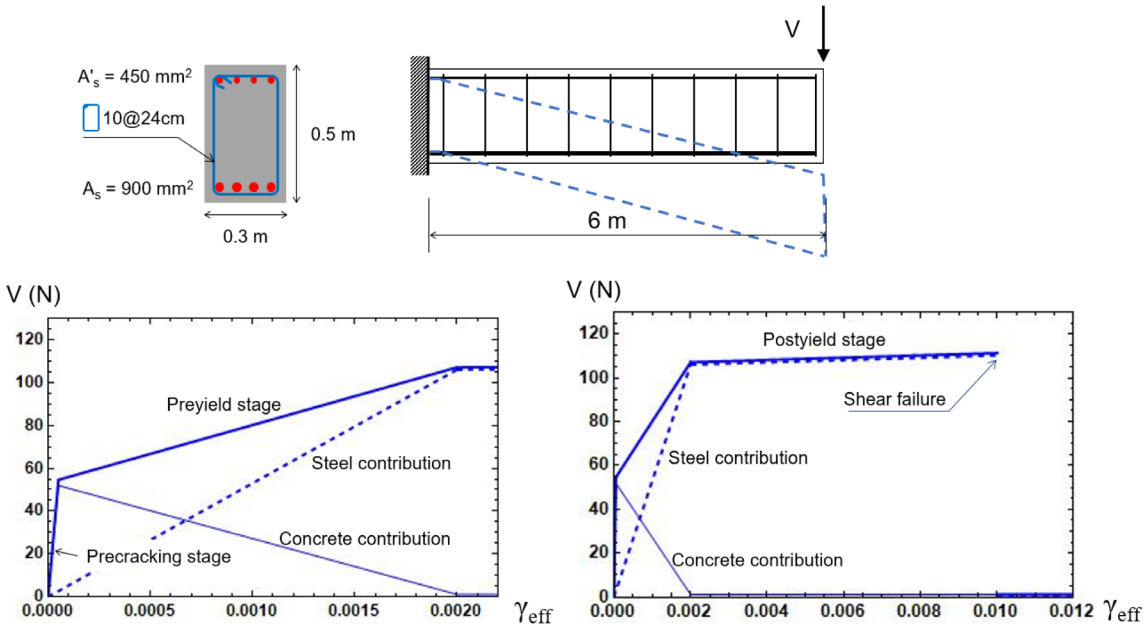

FIGURE 8 Example of a V–γ_{eff} curve.

In order to initiate the algorithm in Figure 7, the initial slopes of both the V–γ_{eff} and moment-curvature curves are used. Additionally, the crack angle (θ) is calculated from Equation (5). This angle can either be kept constant or varied, depending on the compression field theory applied, as mentioned in Section 3.3. Because the moment-curvature graph presents negative slopes for large deformations, the problem is solved by using displacement increments ($\Delta\mathbf{D}$) rather than by using loading increments, with i as the control degree of freedom.

4.1 | Flow chart description

The flowchart in Figure 7 begins with a linear elastic analysis, calculating the displacement vector $\mathbf{D}$ in response to an initial external force vector $\mathbf{F}_0$. The procedure follows a displacement-controlled approach. Figure 7 shows that for each displacement increment $\mathbf{\Delta D_i}$, where $\mathbf{i}$ corresponds to the controlled degree of freedom, the $\mathbf{\Delta F}$ force increment is computed using the stiffness matrix $\mathbf{K}$, i.e., $\mathbf{\Delta F = K\,\Delta D_i}$. Vector $\mathbf{F}$ is obtained by adding the successive $\Delta\mathbf{F}$ to $\mathbf{F_0}$.

Using $\Delta\mathbf{F}$, $\mathbf{K}$, and $\mathbf{K}_B$, the $\Delta\mathbf{D}$ and $\Delta\mathbf{D}_B$ displacement vectors are calculated, with $\Delta\mathbf{D}_B$ as the incremental displacement only caused by bending, and $\Delta\mathbf{D}$ as the incremental displacements caused by bending and shear. The incremental displacement caused by shear, $\Delta\mathbf{D}_S$, is then obtained as the difference between $\Delta\mathbf{D}$ and $\Delta\mathbf{D}_B$. In each step, the $\mathbf{D}$, $\mathbf{D}_B$, and $\mathbf{D}_S$ displacement vectors are obtained from the summation of $\Delta\mathbf{D}$, $\Delta\mathbf{D}_B$, and $\Delta\mathbf{D}_S$, respectively.

For each beam-column element, the curvature and the effective shear strain are obtained from the $\mathbf{d}$, $\mathbf{d}_B$, and $\mathbf{d}_S$ element displacement vectors, which are obtained from the global displacement vectors. The angle of the strut (θ) in each element can be obtained as a function of N, M, and V applied to the element from Equation (5), or from any of the compression field theories.[10] The slopes of the V–γ_{eff} and moment-curvature curves (i.e., α and EI, with $\alpha = GA\kappa_s$ in traditional approaches) are calculated for each value of γ_{eff} and curvature, respectively. Finally, $\mathbf{K}$ and $\mathbf{K}_B$ are updated before the following displacement increment. The procedure has been implemented in Mathematica software.[23]

5 | VALIDATION TEST

In order to validate the RC beam-element presented above, Specimen 7 tested by Tanaka,[24] and studied by Fenves[25] is analyzed here. The properties of the materials are summarized in Table 1. A brief description of the geometry of the specimen is depicted in Figure 9, adapted from page 154 of Reference [24]. The tip of the cantilever is subjected to a compressive axial load (2904 kN) and a variable shear force. Regarding the length of the element, there is a portion near the fixed end ($L_1 = 540$ mm, with the first stirrup located at 30 mm from the fixed end) where the stirrups are more closely spaced (6 stirrups at 90 mm); the rest are spaced at 180 mm. Stirrups are 12 mm diameter and longitudinal bars are 20 mm diameter. The test results are plotted in black in Figure 10.

TABLE 1 Characteristics of materials.

Concrete			Longitudinal reinforcement		Transverse reinforcement	
f_c' (MPa)	E_c (MPa)[26]	f_r (MPa)	f_y (MPa)	f_u (MPa)	f_y (MPa)	f_u MPa)
32	$4700\sqrt{f_c'}$	4	510	675	325	429

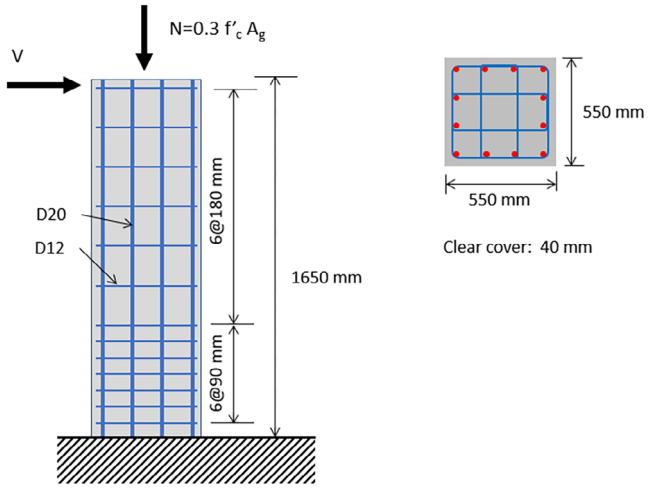

FIGURE 9 Specimen 7 tested by Tanaka.[24,25] Dimensions in mm.

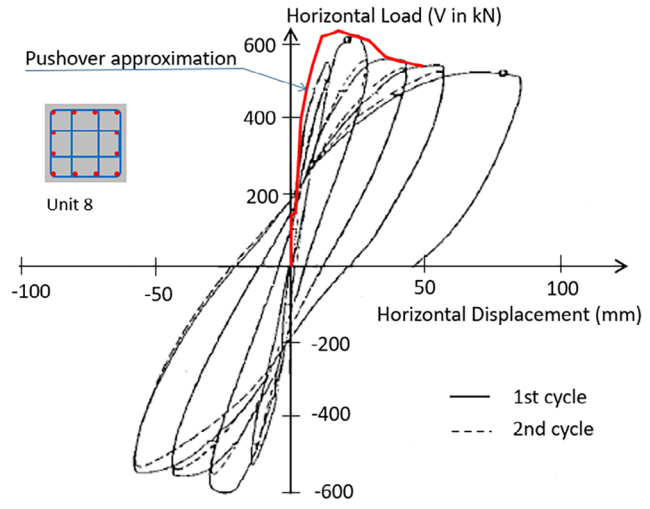

FIGURE 10 Experimental results of the cyclic test of the specimen, adapted from Reference [24] (in black). Monotonic displacement-controlled response using the new RC beam-column element (in red).

The stirrups spaced at 180 mm are intended to withstand the shear force, which remains constant along the length of the column. In contrast, the stirrups spaced at 90 mm are designed to resist shear and to provide confinement to the concrete core. The confinement effect becomes significant only in the lower part of the column, where a substantial bending moment is present.

The specimen is divided into 3 beam-column elements (4 nodes), see Figure 11. Due to the two different separations of the transverse reinforcement, two element types are considered. The longitudinal reinforcement is the same for both element types; however, because of the two different confinements given by the transverse reinforcement, the moment-curvature curves are slightly different (see Figure 11). The calculated response to the monotonic increase in displacement is shown in red in Figure 10. The force–displacement curves tested and calculated align closely up to a shear force of 350 kN. Beyond this point, the discrepancy may be attributed to bond-slip effects. As observed in the test, failure occurs as a result of bending.

According to Equation (5), the crack (or strut) angle is 29.2°. This value is adopted as the strut angle for the red curve in Figure 10 (i.e., $\theta = 29.2°$).

In this study, pushover analyses are performed using both $\theta = 29.2°$ and $\theta = 45°$, with the latter included solely for comparison to highlight the influence of the angle on the response of the RC member. Figure 12 illustrates that the shear-γ_{eff} curves differ for both element types and for the two crack angles considered.

The pushover curves (top displacement versus shear force) corresponding to the specimen studied (see Figure 9) for the two cases considered ($\theta = 29.2°$ and $\theta = 45°$) are shown in Figure 13. For $\theta = 29.2°$, failure occurs as a result of bending. However, for $\theta = 45°$ (blue curve in Figure 13), the stirrups reach the pre-yield state at $V = 280$ kN (see Figures 8 and 13), exhibiting significant shear deformation. The shear reinforcements then enter the post-yield stage at $V = 400$ kN, leading to collapse at a top displacement of 20 mm. The new RC beam-column element captures the potential for both bending and shear failures. In the example analyzed, if the axial force were removed (see line in blue in Figure 13), the structure would exhibit shear failure instead of bending failure.

Figure 12 for $\theta = 29.2°$ shows that at $V = 600$ kN, the transverse reinforcement is at the end of the pre-yield stage for the element type 2, while the concrete is cracked as a result of shear forces (see V–γ_{eff} graphs in Figure 8).

An experimental campaign will soon be conducted to evaluate how accurately the proposed theory reflects real behavior when a set of beam-column elements fail in shear rather than in bending.

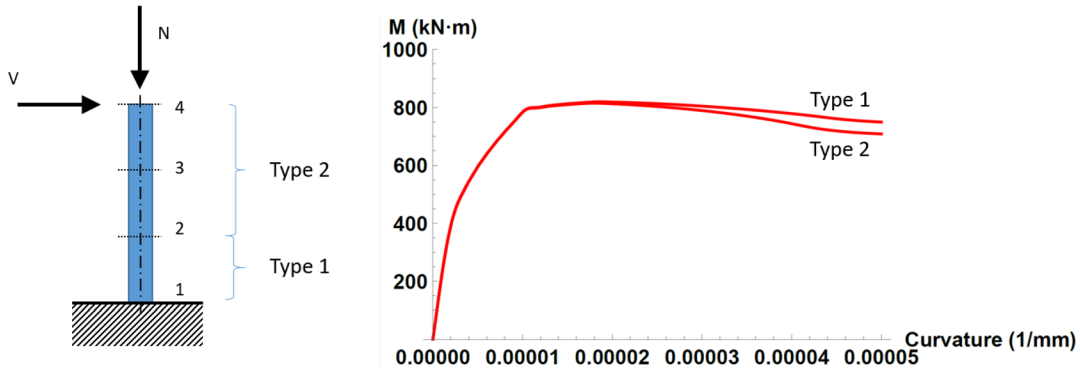

FIGURE 11 Moment-curvature diagrams for the two types of elements.

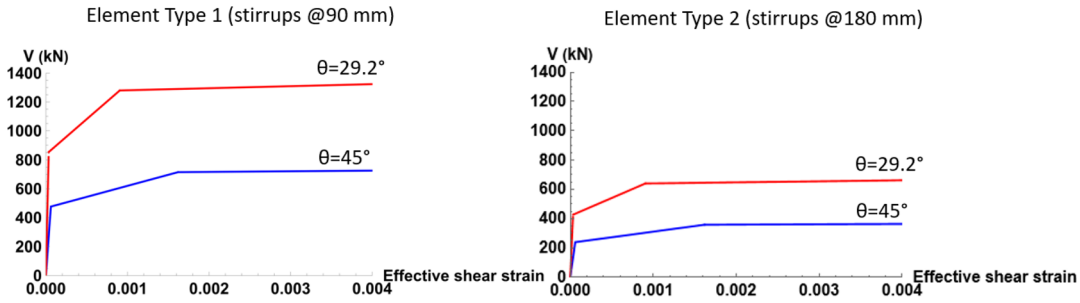

FIGURE 12 Shearing force-effective shear strain curves.

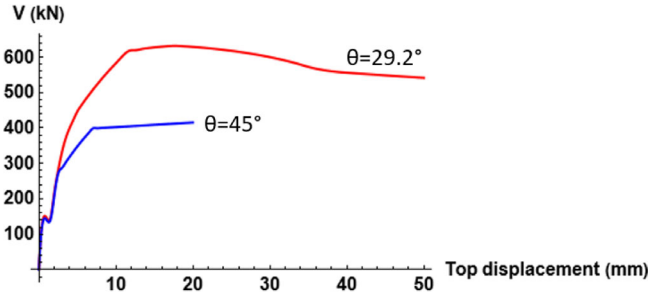

FIGURE 13 Monotonic displacement-controlled response for $\theta = 29.2°$ and $\theta = 45°$.

6 | CONCLUSIONS

Shear deformation in the structural analysis of RC structures has always been considered to be negligible when compared with bending deformation. Nevertheless, shear capacity has to be considered because, due to the short length of transversal reinforcement, maximum strain can be easily reached. In the performance-based design of an RC beam-column, a formulation like the one presented here guarantees that shear failure is detected.

The importance of shear behavior in RC beam-column elements depends on their transverse reinforcement. In certain cases, shear behavior becomes non-negligible and must be considered in structural analyses. Traditionally, shear stiffness (GAk_s) has been assumed to be constant, and shear deformation has been addressed by considering specific displacement and rotation fields that meet the conditions of the system of differential equations used in the TBT. However, given the unique features of RC elements, their shear stiffness cannot be assumed to be constant; in fact, it varies both along the response curve and the length of the element (influenced by the reinforcement layout). This paper has presented a procedure which considers the shear deformation of RC elements in the elastic and plastic domains. The methodology proposed is straightforward and can be easily implemented in fiber element software packages.

NOMENCLATURE

A	cross-section area
$A_{c,eff}$	effective area of concrete or area of concrete contributing to tension stiffening, defined as a rectangular area perpendicular to the bar extending over a distance from the bar smaller than 5.0ϕ
A_s	area of steel
A_ϕ	area of the vertical leg
$\mathbf{d}$, $\mathbf{D}$	total displacements of element and structure
$\mathbf{d}_B$, $\mathbf{D}_B$	displacements of element and structure induced by bending

$\mathbf{d_S}$, $\mathbf{D_S}$	displacements of element and structure induced by shear
ϕ	bar diameter (in mm)
E	modulus of elasticity
E_c	secant modulus of elasticity of concrete
E_s	modulus of elasticity of reinforcing steel
f_c'	compressive strength of concrete
f_{ct}	concrete strength in tension
f_r	modulus of rupture of concrete
f_y	steel yield stress
f_u	steel ultimate stress
$\mathbf{F}$, $\mathbf{F_0}$	force vector, initial force vector
G	shear modulus
I	moment of inertia
$\mathbf{k}$, $\mathbf{K}$	element and structural mechanical stiffness matrix considering shear deformation
$\mathbf{k_B}$, $\mathbf{K_B}$	Bernoulli element and structural mechanical stiffness matrix considering (i.e., not considering shear deformation)
L	length of element
N	axial force
M	bending moment
V	shearing force
n_l	number of legs per stirrup
s	distance between vertical bars
u	longitudinal deflection
v	transverse deflection
z	lever arm
α	shear stiffness, slope of the V–γ curve
β	traditional ratio between flexural and shear stiffnesses
γ	shear rotation, shear strain
γ_{eff}	effective shear strain
Γ_i	integration constants
κ_s	shear correction factor
σ_x	concrete longitudinal stress (in x-axis)
σ_{sv}	stress in vertical reinforcing steel
θ	crack angle and rotation degree of freedom caused by bending

DATA AVAILABILITY STATEMENT

The data that support the findings of this study are available from the corresponding author upon reasonable request.

ORCID

E. Hernández-Montes https://orcid.org/0000-0001-6068-1264

REFERENCES

1. Moehle JP. Displacement-based design of RC structures subject to earthquakes. Earthq Spectra. 1992;8(3):403–28.
2. SEAOC. Vision 2000: Performance based seismic engineering of buildings. 1995.
3. Priestley M. Performance based seismic design. Bull New Zeal Soc Earthq Eng. 2000;33(3):325–46.
4. Orakcal K, Wallace J. Flexural modeling of reinforced concrete walls—experimental verification. ACI Struct J. 2006;103(2):196–206.
5. Kolozvari K, Orakcal K, Wallace JW. New opensees models for simulating nonlinear flexural and coupled shear-flexural behavior of RC walls and columns. Comput Struct. 2018;196:246–62. https://doi.org/10.1016/j.compstruc.2017.10.010
6. Alemdar BN, White DW. Displacement, flexibility, and mixed beam-column finite element formulations for distributed plasticity analysis. J Struct Eng. 2005;131:1811–9.
7. Ramezansefat H, Barros J, Rezazadeh M. A model for the simultaneous prediction of the flexural and shear deflections of statically determinate and indeterminate reinforced concrete structures. Struct Concr. 2017;18(4):618–33. https://doi.org/10.1002/suco.201600116
8. Kolozvari K, Biscombe L, Dashti F, Dhakal RP, Gogus A, Gullu MF, et al. State-of-the-art in nonlinear finite element modeling of isolated planar reinforced concrete walls. Eng Struct. 2019;194:46–65. https://doi.org/10.1016/j.engstruct.2019.04.097
9. Hippola S, Rajapakse C, Mihaylov B, Wijesundara K. A force-based fiber beam-column element to predict moment-axial-shear interaction of reinforced concrete frames. Struct Concr. 2021;22(4):2466–81. https://doi.org/10.1002/suco.202100262
10. Hdz-Gil L, Gil-Martín LM, Hernández-Montes E. A simple method for calculating the shear deformation of reinforced concrete elements in the elastic and plastic domains. Int J Civ Eng. 2023;21:2037–47. https://doi.org/10.1007/s40999-023-00864-y
11. Popovics S. A numerical approach to the complete stress-strain curves for concrete. Cem Concr Res. 1973;3(5):583–99.
12. Mander J, Priestley M, Park R. Theoretical stress-strain model for confined concrete. J Struct Eng. 1988;114(8):1804–26.
13. Timoshenko SP. Strength of materials (part I). 2nd ed. New York: D. Van Nostrand Company, Inc.; 1948.
14. Reddy JN. On locking-free shear deformable beam finite elements. Comput Methods Appl Mech Eng. 1997;149(1–4):113–32. https://doi.org/10.1016/S0045-7825(97)00075-3
15. Ueda T, Sato Y, Ito T, Nishizono K. Shear deformation of reinforced concrete beam. Doboku Gakkai Ronbunshu. 2002;2002(711):205–15. https://doi.org/10.2208/jscej.2002.711_205
16. Hernández-Montes E, Gil-Martín LM. Concrete structures: design and residual capacity assessment. Boca Raton, FL: CRC Press/Taylor & Francis; 2024.
17. Vecchio FJ, Collins MP, Vecchio FJ, Collins MP. The modified compression-field theory for reinforced concrete elements subjected to shear. ACI J. 1986;83(2):219–31.
18. Hsu TTC. Stresses and crack angles in concrete membrane elements. J. Struct. Eng. 1998;124(12):1476–84. https://doi.org/10.1061/(ASCE)0733-9445(1998)124:12(1476)
19. Agarwal A, Foster SJ, Stewart MG. Model error and reliability of reinforced concrete beams in shear designed according to the modified compression field theory. Struct Concr. 2021;22(6):3711–26. https://doi.org/10.1002/suco.202100319
20. Deierlein G, Reinhorn A, Willford M. NEHRP Seismic Design Technical Brief No. 4—Nonlinear Structural Analysis for Seismic Design: A Guide for Practicing Engineers. 2010 [Online].

https://www.nist.gov/publications/nehrp-seismic-design-technical-brief-no-4-nonlinear-structural-analysis-seismic-design
21. prEN 1992-1-1:2013. Eurocode 2: Design of concrete structures - Part 1–1: General rules and rules for buildings, bridges and civil engineering structures EN 1992-1-1. European Committee for Standardization, Brussels 2022.
22. Hdz-Gil L, Hernández-Montes E. Modelo lineal de la rigidez a tracción del hormigón para elementos de hormigón estructural. Hormigon Acero. 2023;74(301):69–74. https://doi.org/10.33586/hya.2023.3097
23. Wolfram Research Mathematica [Software], 2025. https://www.wolfram.com/mathematica/ (Accessed: Mar 03, 2025).
24. Tanaka H. Effect of lateral confining reinforcement on the ductile behaviour of reinforced concrete columns. Ph.D. Thesis 1990.p. 491
25. Scott MH, Fenves GL. Plastic hinge integration methods for force-based beam–column elements. J Struct Eng. 2006;132(2):244–52. https://doi.org/10.1061/(asce)0733-9445(2006)132:2(244)
26. ACI Commitee 318, 318–19. Building Code Requirements for Structural Concrete and Commentary. Detroit: American Concrete Institute. ACI 2019.
27. Reissner E. The effect of transverse shear deformation on the bending of elastic plates. J Appl Mech. 1945;12(2):69–77.
28. Friedman JB, Kosmatka Z. An improved two-node Timoshenko beam finite element. Comput Struct. 1993;47:473–81.

AUTHOR BIOGRAPHIES

L. M. Gil-Martín, Professor, Department of Structural Mechanics, University of Granada (UGR), Campus Universitario de Fuentenueva s/n, 18072 Granada, Spain. Email: mlgil@ugr.es.

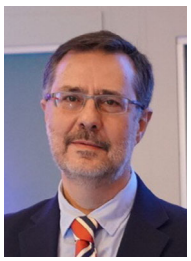

E. Hernández-Montes, Professor, Department of Structural Mechanics, University of Granada (UGR), Campus Universitario de Fuentenueva s/n, 18072 Granada, Spain. Email: emontes@ugr.es.

How to cite this article: Gil-Martín LM, Hernández-Montes E. RC beam-column element for simulating nonlinear shear-flexural behavior. Structural Concrete. 2025. https://doi.org/10.1002/suco.70248

APPENDIX A

A.1 | FINITE ELEMENT FORMULATION OF THE TIMOSHENKO BEAM

Unlike the Euler–Bernoulli beam theory, in which deformation is entirely caused by bending and in-plane stretching, the TBT includes a state of transverse shear strain that is assumed to be constant throughout the thickness of the beam.[13]

Without any loss of generality, a cantilever beam subjected to a uniformly distributed q transverse load[21,22] is considered, based on the following field of displacements (Figure A1):

$$u(x,y) = -y\theta(x) \tag{A1}$$

$$v(x,y) \simeq v(x) \tag{A2}$$

$$\frac{dv(x)}{dx} = \gamma(x) + \theta(x) \tag{A3}$$

where $u(x, y)$ in Equation (A1) is the horizontal displacement of a fiber located at y from the centerline (see red points in Figure A1), and $v(x)$ in Equation (A2) is the transverse deflection of the centerline of the beam. Figure A1 shows that the x-coordinate is taken along the length of the beam. All the points in the same cross-section are assumed to have the same displacements in the y-axis. In the expressions above, $\theta(x)$ is the rotation caused by bending, or the angle of the centerline with the x-axis induced by bending, and $\gamma(x)$ is the shear strain (that is, the angle of the centerline with the x-axis caused by the shear deformation), as shown in Figure A1. Therefore, the angle of the centerline (i.e., $dv(x)/dx$) is the summation of bending and shearing effects, Equation (A3). Equations (A1) and (A2) are also present in the Bernoulli beam formulation, and Equation (A3) characterizes the Timoshenko beam.

Establishing the balance of internal moments and transverse forces, assuming linear elasticity:

$$\begin{aligned} M(x) &= \int_A y\sigma_x dA = \int_A yE\varepsilon_x dA = \int_A yE\frac{\partial u}{\partial x}dA \\ &= -\int_A Ey^2\frac{d\theta(x)}{dx}dA = -EI\frac{d\theta(x)}{dx} \end{aligned} \tag{A4}$$

$$\begin{aligned} V(x) &= \int_A \tau dA = \int_A G\gamma dA = \kappa_s\int_A G\left(\frac{dv(x)}{dx} - \theta(x)\right)dA \\ &= GA\kappa_s\left(\frac{dv(x)}{dx} - \theta(x)\right) \end{aligned} \tag{A5}$$

with G as the shear modulus, τ as the average shear stress, and κ_s as a shear correction factor to compensate for the error caused by the assumption of constant shear stress (and strain) on the beamcross-section ($\kappa_s = 5/6$ for

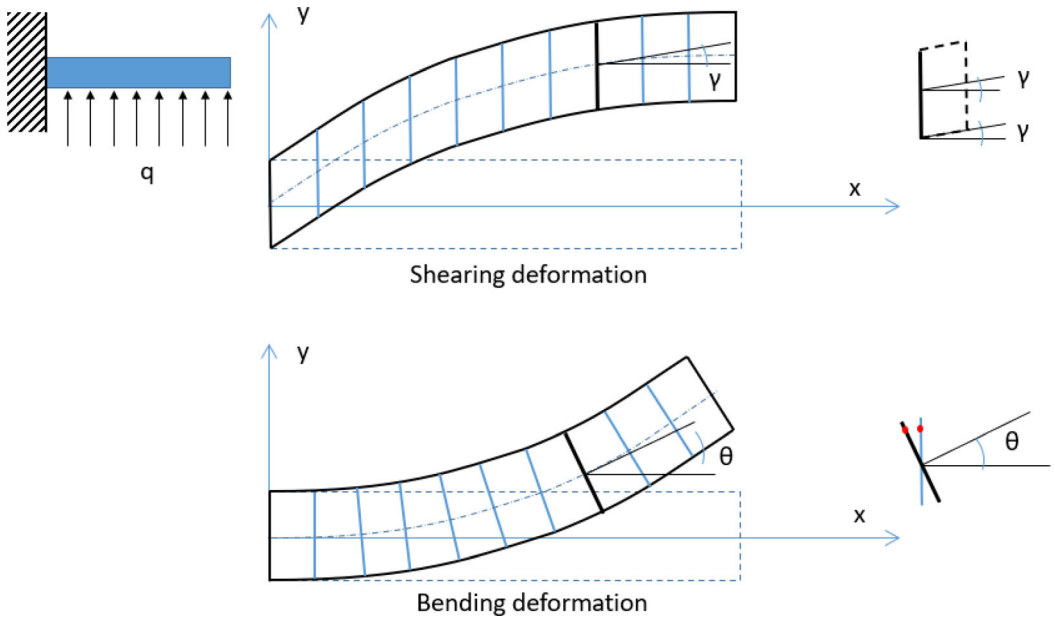

FIGURE A1 Displacement field of the TBT.

rectangular cross sections[27]). In Equation (A5), a constant state of transverse shear strain throughout the thickness of the beam is assumed.

For the purpose of derivation, both EI and $GA\kappa_s$ are assumed to be constant. Note that both terms can be assumed to be constant in incremental studies when considering small enough increments of loading.

Considering equilibrium of moments and transverse forces over a segment of beam:

$$\frac{dM(x)}{dx} - V(x) = 0 \rightarrow EI\theta''(x) + GA\kappa_s(v'(x) - \theta(x)) = 0 \tag{A6}$$

$$\frac{dV(x)}{dx} = -q \rightarrow GA\kappa_s(v''(x) - \theta'(x)) = -q \tag{A7}$$

The two second-order coupled equations, Equations (A6) and (A7), are the governing equations of the TBT. The solution for the system of differential equations is:

$$v(x) = -\frac{qx^2}{2GA\kappa_s} + \frac{qx^4}{24EI} - \frac{EI}{GA\kappa_s}\Gamma_1 x + \left(\frac{\Gamma_1}{6}x^3 + \frac{\Gamma_2}{2}x^2 + \Gamma_3 x + \Gamma_4\right) \tag{A8}$$

$$\theta(x) = \frac{qx^3}{6EI} + \frac{\Gamma_1}{2}x^2 + \Gamma_2 x + \Gamma_3 \tag{A9}$$

with Γ_i as integration constants depending on the boundary conditions of the problem.

Normally,[28] the element finite formulation is based on shape functions for v and θ, which are determined using the exact homogeneous form of the equilibrium equations of a Timoshenko beam subjected to a uniformly distributed transverse load[14] (i.e., placing $q = 0$ in Equation (A7)). The displacement and rotation field solutions for the homogeneous system of equations are those indicated in Equations (A8) and (A9), that is:

$$v(x) = -\frac{EI}{GA\kappa_s}\Gamma_1 x + \left(\frac{\Gamma_1}{6}x^3 + \frac{\Gamma_2}{2}x^2 + \Gamma_3 x + \Gamma_4\right) \tag{A10}$$

$$\theta(x) = \frac{\Gamma_1}{2}x^2 + \Gamma_2 x + \Gamma_3 \tag{A11}$$

If the displacement and rotation fields in Equations (A10) and (A11) are adopted,[14] then a constant state of transverse shear strain is obtained:

$$\gamma(x) = v'(x) - \theta(x) = -\frac{EI}{GA\kappa_s}\Gamma_1 \tag{A12}$$

For a two-node beam, the above fields can be expressed in matrix form as:

$$\begin{Bmatrix} v(x) \\ \theta(x) \end{Bmatrix} = \mathbf{P}\boldsymbol{\Gamma}$$
$$\text{with: } \mathbf{P} = \begin{pmatrix} x^3/6 - x\beta & x^2/2 & x & 1 \\ x^2/2 & x & 1 & 0 \end{pmatrix} \tag{A13}$$
$$\boldsymbol{\Gamma}^T = \{\Gamma_1, \Gamma_2, \Gamma_3, \Gamma_4\}$$
$$\beta = \frac{EI}{GA\kappa_s}$$

And the transverse nodal displacements and rotations can be obtained as (see Figure 3 in the paper):

$$\boldsymbol{\delta}^T = \{v_1, \theta_1, v_2, \theta_2\}$$

with :

$$\begin{aligned} v_1 &= v(0) \\ \theta_1 &= \theta(0) \\ v_2 &= v(L) \\ \theta_2 &= \theta(L) \end{aligned} \tag{A14}$$

with L as the length of the beam element. Equation (A14) can be rewritten in matrix form as:

$$\boldsymbol{\delta} = \mathbf{C}\boldsymbol{\Gamma} \text{ with } \mathbf{C} = \begin{pmatrix} 0 & 0 & 0 & 1 \\ 0 & 0 & 1 & 0 \\ L^3/6 - \beta L & L^2/2 & L & 1 \\ L^2/2 & L & 1 & 0 \end{pmatrix} \tag{A15}$$

Considering Equations (A13) and (A15), the following equality is obtained:

$$\begin{Bmatrix} v(x) \\ \theta(x) \end{Bmatrix} = \mathbf{P}\boldsymbol{\Gamma} = \mathbf{P}\mathbf{C}^{-1}\boldsymbol{\delta} = \mathbf{N}\boldsymbol{\delta} \tag{A16}$$

with :

$$\mathbf{N} = \frac{1}{L(L^2+12\beta)} \begin{pmatrix} (L-x)\left(L^2+Lx-2x^2+12\beta\right) & (L-x)x\left(L^2-Lx+6\beta\right) & x\left(3Lx-2x^2+12\beta\right) & -(L-x)x(Lx+6\beta) \\ 6x(-L+x) & (L-x)\left(L^2-3Lx+12\beta\right) & 6x(-L+x) & x\left(-2L^2+3Lx+12\beta\right) \end{pmatrix}$$

With $\mathbf{N}$ as the shape function matrix (Hermite cubic shape function matrix if β tends to 0, or equivalently, if shear stiffness $GA\kappa_s$ tends to infinity).

Considering the above expressions, the bending curvature of the beam and the shear strain can be written as:

$$\begin{Bmatrix} \phi \\ \gamma \end{Bmatrix} = \begin{Bmatrix} \theta'(x) \\ v'(x) - \theta(x) \end{Bmatrix} = \mathbf{Q}\boldsymbol{\Gamma} = \mathbf{Q}\mathbf{C}^{-1}\boldsymbol{\delta} = \mathbf{B}\boldsymbol{\delta}$$

$$\text{with : } \mathbf{Q} = \begin{pmatrix} x & 1 & 0 & 0 \\ -\beta & 0 & 0 & 0 \end{pmatrix}$$

$$\text{and } \mathbf{B} = \frac{1}{L(L^2+12\beta)} \begin{pmatrix} -6(L-2x) & -2\left(2L^2-3Lx+6\beta\right) & 6(L-2x) & -2\left(L^2-3Lx-6\beta\right) \\ -12\beta & -6\beta L & 12\beta & -6\beta L \end{pmatrix} \tag{A17}$$

By applying the virtual work principle, the stiffness matrix of an element with constant values of EI and $GA\kappa_s$ is obtained as:

$$\boldsymbol{k} = \int_L B^T \begin{pmatrix} \mathrm{EI} & 0 \\ 0 & GA\kappa_s \end{pmatrix} \mathbf{B}\, dx = \frac{2\mathrm{EI}}{L^3(1+12\beta/L^2)} \begin{pmatrix} 6 & 3L & -6 & 3L \\ 3L & 2L^2+6\beta & -3L & L^2-6\beta \\ -6 & -3L & 6 & -3L \\ 3L & L^2-6\beta & -3L & 2L^2+6\beta \end{pmatrix} \tag{A18}$$

In the previous development, axial force was ignored. If the DOF in Figure 3 are considered, $\mathbf{k}$ can be extended to the well-known stiffness matrix of a beam-column element:

$$\begin{Bmatrix} N_i \\ V_i \\ M_i \\ N_j \\ V_j \\ M_j \end{Bmatrix} = \begin{bmatrix} \frac{AE}{L} & 0 & 0 & -\frac{AE}{L} & 0 & 0 \\ 0 & \frac{12\mathrm{EI}}{L^3+12L\beta} & \frac{6\mathrm{EI}}{L^2+12\beta} & 0 & -\frac{12\mathrm{EI}}{L^3+12L\beta} & \frac{6\mathrm{EI}}{L^2+12\beta} \\ 0 & \frac{6\mathrm{EI}}{L^2+12\beta} & \frac{4\mathrm{EI}(L^2+3\beta)}{L^3+12L\beta} & 0 & -\frac{6\mathrm{EI}}{L^2+12\beta} & \frac{2\mathrm{EI}(L^2-6\beta)}{L^3+12L\beta} \\ -\frac{AE}{L} & 0 & 0 & \frac{AE}{L} & 0 & 0 \\ 0 & -\frac{12\mathrm{EI}}{L^3+12L\beta} & -\frac{6\mathrm{EI}}{L^2+12\beta} & 0 & \frac{12\mathrm{EI}}{L^3+12L\beta} & -\frac{6\mathrm{EI}}{L^2+12\beta} \\ 0 & \frac{6\mathrm{EI}}{L^2+12\beta} & \frac{2\mathrm{EI}(L^2-6\beta)}{L^3+12L\beta} & 0 & -\frac{6\mathrm{EI}}{L^2+12\beta} & \frac{4\mathrm{EI}(L^2+3\beta)}{L^3+12L\beta} \end{bmatrix} \cdot \begin{bmatrix} u_i \\ v_i \\ \theta_i \\ u_j \\ v_j \\ \theta_j \end{bmatrix} = \mathbf{kd} \tag{A19}$$

If $\beta = 0$, the shearing effect is not considered, and $\mathbf{k}$ is the traditional matrix based on the Bernoulli beam theory ($\mathbf{k}_B$).